Neutrino Nonstandard Interactions and Lepton Flavor Universality violation at SND@LHC via charm production

Bhubanjyoti Bhattacharya ⓘ,[a] **Alakabha Datta** ⓘ,[b] **Elena Graverini** ⓘ,[c,d] **Lopamudra Mukherjee** ⓘ,[e] **Divya Sachdeva,**[f,g] **and John Waite**[h]

[a] *Department of Natural Sciences, Lawrence Technological University, Southfield, MI 48075, USA*

[b] *Department of Physics and Astronomy, 108 Lewis Hall, University of Mississippi, Oxford, MS38677-1848, USA*

[c] *Università di Pisa, Italy*

[d] *École Polytechnique Fédérale, Lausanne, Switzerland*

[e] *School of Physics, Nankai University, Tianjin 300071, China*

[f] *Laboratoire de Physique de l'École normale supérieure, ENS, Université PSL, CNRS, Sorbonne Université, Université Paris Cité, 24 Rue Lhomond, F-75005 Paris, France*

[g] *Indian Institute of Technology Hyderabad, Kandi, Sangareddy-502285, Telangana, India*

[h] *Morehead State University, Morehead, KY, USA*

E-mail: bbhattach@ltu.edu, datta@phy.olemiss.edu, elena.graverini@cern.ch, lopamudra.physics@gmail.com, divyasachdeva@phy.iith.ac.in, j.waite@moreheadstate.edu

ABSTRACT: In this work, we explore the effect of neutrino nonstandard interactions (NSI) involving the charm quark at SND@LHC. Using an effective description of new physics in terms of four-fermion operators involving a charm quark, we constrain the Wilson coefficients of the effective interaction from two and three-body charmed meson decays. In our fit, we include charmed meson decays not only to pseudoscalar final states but also to vector final states and include decays to the η and η' final states. We also consider constraints from charmed baryon decays. We then study the effect of new physics in neutrino scattering processes, involving charm production at SND@LHC, for various benchmark new physics couplings obtained from the low energy fits. Finally, we also study the effects of lepton universality violation (LUV) assuming that the new physics coupling is not lepton universal.

Contents

1 Introduction

The observation of neutrino masses and mixing indicate physics beyond the Standard Model (SM). Therefore, it is reasonable to hypothesize that neutrinos may have new interactions beyond the SM. These interactions, known as neutrino nonstandard interactions (NSI), can be explored in specific models or in a model-independent framework in terms of four-fermion operators. The interactions may be purely leptonic or semileptonic where in the latter case a quark current and a leptonic current are involved in the effective interaction. In typical neutrino experiments, NSI involving the first-generation quarks are involved. In many models of BSM physics, the new physics (NP) effects are more pronounced in the heavier generations. NSI involving the heavy quarks and leptons are particularly interesting in these models. Also, given that there are hints of NP in decays of heavy quarks, a program to explore NSI involving heavy quarks is quite compelling. New high-energy neutrino scattering experiments that will produce charm quarks offer a unique opportunity to study NSI with heavy quarks.

The SM is lepton-flavor universal, i.e. the electroweak gauge interactions of the SM apply identically to all three flavors of leptons. Violation of this universality, known as

lepton universality violation (LUV), is a crucial test of the SM. Evidence of LUV in B-mesons decays has generated significant interest in testing for LUV in various decays. In B decays, hints of LUV have been observed in the charged-current quark-level transition $b \to c\ell^-\bar{\nu}$, where ℓ can be an e, μ, or τ. At the mesonic level, since the hadronic part of such a decay rate is plagued by uncertainties from form factors and the non-perturbative nature of QCD, one considers ratios of decay rates as relatively cleaner tests for LUV.

The SM predictions for the ratios $R_{D^{(*)}}^{\tau/\ell} \equiv \mathcal{B}(\bar{B} \to D^{(*)}\tau^-\bar{\nu}_\tau)/\mathcal{B}(\bar{B} \to D^{(*)}\ell^-\bar{\nu}_\ell)$ (here $\ell = e, \mu$) and $R_{J/\psi}^{\tau/\mu} \equiv \mathcal{B}(B_c^+ \to J/\psi\tau^+\nu_\tau)/\mathcal{B}(B_c^+ \to J/\psi\mu^+\nu_\mu)$ are known to within 2% and 20% respectively [1]. The BaBar, Belle, and LHCb experiments have measured $R_{D^{(*)}}^{\tau/\ell}$ [2–15] and $R_{J/\psi}^{\tau/\mu}$ [16] with a precision of 5-8% and 35% respectively. These measurements currently display some tension with their corresponding SM expectations. In particular, the combined deviation from the SM in $R_{D^{(*)}}^{\tau/\ell}$ is 3.31σ [17], while in $R_{J/\psi}^{\tau/\mu}$ the deviation is 1.7σ. Together these measurements provide strong hints of LUV NP in $b \to c\tau^-\bar{\nu}_\tau$ decays.

Current experimental measurements also allow a 3-5% LUV in the ratio $R_{D^{(*)}} \equiv \mathcal{B}(\bar{B} \to D^{(*)}\mu^-\bar{\nu}_\mu)/\mathcal{B}(\bar{B} \to D^{(*)}e^-\bar{\nu}_e)$, which is expected to be ~ 1 in the SM. For the interested reader, we summarize the SM predictions for these observables and their experimental measurements in Appendix A.

Hints of NP are not restricted to charged-current B decays. A recent first measurement of the branching ratio $\mathcal{B}(B^+ \to K^+\nu\bar{\nu}) = (2.3 \pm 0.7) \times 10^{-5}$ by the Belle II experiment [18] is 2.7σ higher than the SM expectation $\mathcal{B}(B^+ \to K^+\nu\bar{\nu})_{\rm SM} = (5.58 \pm 0.38) \times 10^{-6}$ [19]. Furthermore, even though the recently updated measurements of $R_{K^{(*)}} = \mathcal{B}(B \to K^{(*)}\mu^+\mu^-)/\mathcal{B}(B \to K^{(*)}e^+e^-)$ are now fully consistent with their SM expectations [20], the individual branching fractions in both the electron and muon channels remain discrepant [21]). Joint explanations of all these anomalies, both in model-dependent as well as model-independent approaches, favor NP that affects the heavier generations of quarks and leptons (see for example Refs. [22, 23].)

While many of these anomalies have been observed in low-energy data, if NP is involved, it should also affect quark-lepton interactions at higher energy scales. In this paper, we study the effects of NP, specifically in the neutrino-quark scattering process $\nu_\ell + q \to q' + \ell^-$ where ℓ can be e, μ, or τ. The effects of LUV NP in the scattering of ν_τ off light quarks were studied in Refs. [24–26]. The parameter space of NP couplings and energy scales for ν_τ scattering off light quarks can be constrained using data from hadronic tau decays. However, since the light leptons do not decay hadronically, similar constraints do not appear for ν_e and ν_μ. Instead, if the scattering of ν_ℓ off of a light quark (q) produces a heavy quark (h) then the corresponding parameter space can be constrained by studying semileptonic transitions of a heavy quark to a light quark, $h \to q\ell^-\bar{\nu}$.

Two recently started experiments that can facilitate the exploration of neutrino-quark scattering processes are FASERν [27] and the Scattering and Neutrino Detector at the Large Hadron Collider (SND@LHC) [28]. Both detectors have been designed to investigate the scattering of high-energy neutrinos produced in the far-forward direction at the LHC, specifically at the ATLAS interaction point. In this work, we focus on the physics reach of the SND@LHC experiment. A recent analysis of NSI at FASERν can be found in Ref. [29].

Neutrinos reaching the SND@LHC detector are energetic enough to produce heavy quarks, such as the charm quark, in the final state. This allows SND@LHC to be a laboratory for testing LUV effects in quark-neutrino scattering processes involving a heavy quark. The SND@LHC detector also aims at exploring the possibility of detecting new particles that scatter similar to neutrinos, such as light dark matter (LDM) particles which interact with SM particles through portal mediators. This study focuses on estimating the sensitivity of the SND@LHC detector in detecting new-physics phenomena, considering various benchmark new-physics couplings derived from low-energy fits.

The SND@LHC detector comprises a target region followed by the muon system. The detector pseudorapidity range spans from 7.2 to 8.4. The target consists of five walls of emulsion cloud chambers (ECC) followed by planes of Scintillating Fiber (SciFi) trackers. Each wall comprises 60 emulsion films interleaved with 59 tungsten plates, each 1 mm thick, serving as the target material. The ECC provides micrometric accuracy for measuring charged-particle tracks and reconstructing vertices of neutrino interactions. The reconstruction of particles and showers spanning several emulsion bricks is aided by the interleaved layers of SciFi, that provide accurate time stamps. When combined with the ECC walls used as radiators, the SciFi detector also serves as a sampling calorimeter to measure the energy of electromagnetic showers. Hadronic showers start developing in the target volume, but then they are fully contained by a hadronic calorimeter composed of alternating layers of 20 cm thick iron walls and 1 cm thick scintillating bars.

A key feature of SND@LHC is its high efficiency in identifying neutrino flavors. Electron neutrinos can be identified via their electromagnetic showers with 99% efficiency. Charged-current muon neutrino interactions can be detected with 69% efficiency by requiring the presence of at least one muon track. Neutral current interactions are correctly tagged with 99% efficiency. Thanks to the micrometric resolution of the ECC, tau neutrinos can be identified via a decay vertex that is displaced from the primary interaction point. The ν_τ detection efficiency for SND@LHC ranges from 48% to 54% depending on the decay mode of the τ lepton [28, 30].

In this work, we will explore LUV effects in the scattering process $\nu_\ell + q \to c + \ell^-$ at SND@LHC, where q represents down-type quarks in the target (tungsten) nuclei. The incoming neutrinos are highly energetic so deep-inelastic scattering (DIS) is the underlying process. In the SM, the contributions from a b-quark in the initial state are suppressed due to the relative smallness of the Cabibbo-Kobayashi-Maskawa (CKM) matrix element V_{cb} compared to contributions from a d or s quark in the initial state. For the same reason, the scattering process where an up-type quark from the target nuclei contributes in the initial state to produce a b quark in the final state is also suppressed and is not considered here. We adopt an effective field theory (EFT) framework starting with all dimension 6 operators that can contribute to the process. We then constrain the Wilson Coefficients (WCs) of the effective operators using low-energy measurements of two- and three-body D decays. While constraints on NP from semileptonic charmed mesons have been considered before [31], here we present a more exhaustive fit to the low-energy charm semileptonic decays. In our low-energy observables, we consider both two-body leptonic and three-body semileptonic decays of charmed mesons where we include decays not only to pseudoscalar

final states but also to vector final states and include in our fits decays to the η and η' mesons. We also consider constraints from charmed baryon decays. After the low energy fit, various benchmark values for the WCs are then used to study the prospects of detecting NP at SND@LHC. Although our results are specifically derived for the case of SND@LHC, they can be easily adapted and rescaled for application to FASERν.

The paper is organized in the following manner. In section II, we describe the formalism of the effective Hamiltonian and discuss several UV complete models from which the effective operators in the Hamiltonian can emerge. In section III, we discuss the low-energy flavor observables, perform fits to constrain the WCs, and choose benchmark values for the neutrino scattering study. In section IV, we consider the neutrino scattering and discuss the level of significance at which LUV effects can be detected at SND@LHC. We summarize and present our conclusions in section V.

2 Effective Hamiltonian

We begin by considering an effective Hamiltonian with dimension 6 four-fermion operators and Wilson coefficients that encode high-energy NP. Using the effective Hamiltonian we choose benchmark values for Wilson coefficients using constraints from low-energy observables including leptonic and semileptonic decays of D mesons. The benchmark values are then used to study the effects of NP on neutrino scattering. The effective Hamiltonian that contributes to the scattering process $\nu_\ell + q \rightarrow c + \ell^-$ can be expressed as [29, 32]:

$$
H_{\text{eff}} = \frac{4 G_F V_{cq}}{\sqrt{2}} \left\{ (1 + \epsilon_L)_{\alpha\beta} [\bar{c}\gamma_\mu P_L q][\bar{\ell}_\alpha \gamma^\mu P_L \nu_\beta] + (\epsilon_R)_{\alpha\beta} [\bar{c}\gamma_\mu P_R q][\bar{\ell}_\alpha \gamma^\mu P_L \nu_\beta] \right.
$$
$$
+ (\epsilon_S)_{\alpha\beta} [\bar{c}q][\bar{\ell}_\alpha P_L \nu_\beta] + (\epsilon_P)_{\alpha\beta} [\bar{c}\gamma^5 q][\bar{\ell}_\alpha P_L \nu_\beta]
$$
$$
\left. + (\epsilon_T)_{\alpha\beta} [\bar{c}\sigma_{\mu\nu} P_L q][\bar{\ell}_\alpha \sigma^{\mu\nu} P_L \nu_\beta] \right\} + \text{ h.c.,} \quad (2.1)
$$

where α, β are lepton flavor indices representing the three flavors e, μ, and τ, and $q = s, d$. Here P_R and P_L are respectively the right and left projection operators $(1 \pm \gamma^5)/2$, G_F refers to the Fermi constant, V_{cq} refers to the appropriate CKM matrix element, and $(\epsilon_X)_{\alpha\beta}$ refer to the NP Wilson coefficients where X can be L, R, S, P, or T for left-handed vector, right-handed vector, scalar, pseudoscalar, or tensor. Here the neutrinos are left-handed Dirac particles and X refers to the Lorentz structure of the quark current.

To obtain benchmarks for $(\epsilon_X)_{\alpha\beta}$ we will study processes where the quark-level transition is of the type $(\bar{c}q)(\bar{\ell}\nu)$, specifically two- and three-body decays of D and D^* mesons. Now, since neutrinos are not directly detected at collider experiments the final state neutrino flavor in a two- or three-body meson decay is unknown. Any effect of neutrino flavor gets washed out in summing over the final-state neutrino flavor. While in principle NSI can lead to lepton flavor violation when $(\epsilon_X)_{\alpha\beta}$ is nonzero for $\alpha \neq \beta$, here we will always sum over the neutrino flavor index β. The resulting Hamiltonian is effectively flavor diagonal and can be expressed as

$$
H_{\text{eff}} = \frac{4 G_F V_{cq}}{\sqrt{2}} \left\{ (1 + \epsilon_L)[\bar{c}\gamma_\mu P_L q][\bar{\ell}\gamma^\mu P_L \nu] + \epsilon_R [\bar{c}\gamma_\mu P_R q][\bar{\ell}\gamma^\mu P_L \nu] \right.
$$
$$
\left. + \epsilon_S [\bar{c}q][\bar{\ell}_\alpha P_L \nu_\beta] + \epsilon_P [\bar{c}\gamma^5 q][\bar{\ell} P_L \nu] + \epsilon_T [\bar{c}\sigma_{\mu\nu} P_L q][\bar{\ell}\sigma^{\mu\nu} P_L \nu] \right\} + \text{ h.c.,} \quad (2.2)
$$

where without the loss of generality here and in what follows we have suppressed the charge-lepton flavor index α on the effective WCs ϵ_X ($X = L, R, S, P, T$) obtained after summing over the neutrino flavor index β,

$$\epsilon_X^\alpha \;=\; \sum_\beta^{e, \mu, \tau} (\epsilon_X)_{\alpha\beta} \; . \tag{2.3}$$

It is common to use a different nomenclature and basis of WCs, especially for the scalar and pseudoscalar operators which can instead be written in terms of left- and right-handed operators. This is done by rewriting the above Hamiltonian as follows

$$H_{\text{eff}} = \frac{4 G_F V_{cq}}{\sqrt{2}} \left\{ (1 + V_L)[\bar{c}\gamma_\mu P_L q][\bar{\ell}\gamma^\mu P_L \nu] + V_R[\bar{c}\gamma_\mu P_R q][\bar{\ell}\gamma^\mu P_L \nu] \right.$$
$$\left. + S_L[\bar{c}P_L q][\bar{\ell}P_L \nu] + S_R[\bar{c}P_R q][\bar{\ell}P_L \nu] + T_L[\bar{c}\sigma_{\mu\nu}P_L q][\bar{\ell}\sigma^{\mu\nu}P_L \nu] \right\} \; + \; \text{h.c.,} \tag{2.4}$$

where X_Y represent the effective NP WCs with $X = S, V, T$ referring to scalar, vector, or tensor and $Y = L, R$ referring to left-handed and right-handed quark currents. We have once again suppressed the charged-lepton flavor index, α, in Eq. (2.4). By comparing Eqs. (2.2) and (2.4) one can relate the two sets of WCs as follows,

$$V_{L(R)} \;=\; \epsilon_{L(R)} \;, \quad S_L \;=\; \epsilon_S - \epsilon_P \;, \quad S_R \;=\; \epsilon_S + \epsilon_P \;. \quad T_L \;=\; \epsilon_T \;, \tag{2.5}$$

Thus, constraints from meson decay experiments can be directly translated into bounds on five WCs, $V_L, V_R, S_L, S_R,$ and T_L for each lepton flavor $e, \mu,$ and τ.

The effective Hamiltonian given in Eq. (2.4) above can come from various ultraviolet-complete models. We discuss two specific examples – the leptoquark model and the vector boson (W') model. Here we demonstrate how the Wilson coefficients in Eq. (2.4) can be expressed in terms of tree-level couplings within these ultraviolet-complete models.

The interaction of a singlet leptoquark, $S_1(\bar{3}, 1, 1/3)$, with SM fermions can be expressed as [33],

$$\mathcal{L}^{\text{LQ}} = \left(g_{1L}^{ij} \, \bar{Q}_{iL}^c i\sigma_2 L_{jL} + g_{1R}^{ij} \, \bar{u}_{iR}^c \ell_{jR} \right) S_1 \; + \; \text{h.c.,} \tag{2.6}$$

where Q_i and L_j represent the left-handed quark and lepton doublets, u_{iR} and d_{iR} are the right-handed up-type and down-type quark singlets and ℓ_{jR} represents the right-handed charged lepton singlets. Indices i and j denote the generations of quarks and leptons. Integrating out the heavy S_1 leptoquark one obtains the following effective operators involving neutrinos.

$$\mathcal{L}_{\text{eff}}^{(1)} \;=\; \frac{g_{1L}^{ij} g_{1L}^{kl*}}{M_{S_1}^2} \left(\bar{Q}_{iL}^c \sigma_2 L_{jL} \right) \left(\bar{L}_{kL} \sigma_2 Q_{lL}^c \right), \tag{2.7}$$

$$\mathcal{L}_{\text{eff}}^{(2)} \;=\; \frac{g_{1L}^{ij} g_{1R}^{kl*}}{M_{S_1}^2} \left(\bar{Q}_{iL}^c i\sigma_2 L_{jL} \right) \left(\bar{\ell}_{lR} u_{kR}^c \right) \; + \; \text{h.c.,} \tag{2.8}$$

$$\;=\; \frac{g_{1L}^{ij} g_{1R}^{kl*}}{M_{S_1}^2} \left\{ \left(\bar{u}_{iL}^c \ell_{jL} \right) \left(\bar{\ell}_{lR} u_{kR}^c \right) - \left(\bar{d}_{iL}^c \nu_{jL} \right) \left(\bar{\ell}_{lR} u_{kR}^c \right) \right\} \; + \; \text{h.c.} \tag{2.9}$$

After a Fierz transformation, $\mathcal{L}_{\text{eff}}^{(1)}$ can be written as

$$\mathcal{L}_{\text{eff}}^{(1)} = \frac{g_{1L}^{ij}g_{1L}^{kl*}}{4M_{S_1}^2}\left[\left(\bar{Q}_{kL}\gamma^\mu Q_{iL}\right)\left(\bar{L}_{lL}\gamma_\mu L_{jL}\right) - \left(\bar{Q}_{kL}\gamma^\mu\sigma^I Q_{iL}\right)\left(\bar{L}_{lL}\gamma_\mu\sigma^I L_{jL}\right)\right]. \quad (2.10)$$

Only the second term above contains lepton-neutrino interactions which can be expressed using the following effective Hamiltonian.

$$\mathcal{H}_{\text{eff}}^{(1)} = -\frac{g_{1L}^{2l}g_{1L}^{2l*}}{2M_{S_1}^2}\left(\bar{c}\gamma^\mu P_L s\right)\left(\bar{\ell}\gamma_\mu P_L \nu\right) + \text{ h.c.} \quad (2.11)$$

In a similar vein, the second of the two terms in $\mathcal{L}_{\text{eff}}^{(2)}$, after Fierz transformation, gives rise to the following effective Hamiltonian,

$$\mathcal{H}_{\text{eff}}^{(2)} = -\frac{g_{1L}^{2l}g_{1R}^{2l*}}{2M_{S_1}^2}\left[\left(\bar{c}P_L s\right)\left(\bar{\ell}P_L \nu\right) + \frac{1}{4}\left(\bar{c}\sigma^{\mu\nu}P_L s\right)\left(\bar{\ell}\sigma_{\mu\nu}P_L \nu\right)\right] + \text{ h.c.} \quad (2.12)$$

Comparing the above effective Hamiltonians with that of Eq. (2.4) and restricting ourselves to second-generation quarks, we can express the coefficients S_L, V_L, and T_L as follows,

$$S_L = -\frac{1}{2\sqrt{2}G_F V_{cs}}\frac{g_{1L}^{2l}g_{1R}^{2l*}}{2M_{S_1}^2}, \quad V_L = \frac{1}{2\sqrt{2}G_F V_{cs}}\frac{g_{1L}^{2l}g_{1L}^{2l*}}{2M_{S_1}^2}, \quad T_L = -\frac{1}{2\sqrt{2}G_F V_{cs}}\frac{g_{1L}^{2l}g_{1R}^{2l*}}{8M_{S_1}^2}. \quad (2.13)$$

Let us now consider the following Lagrangian, encoding the interaction of a W' boson with leptons and quarks:

$$\mathcal{L}^{W'} = \frac{g}{\sqrt{2}}\left[V_{ij}\left\{\bar{u}_i\gamma^\mu(g_L^{ij}P_L + g_R^{ij}P_R)d_j\right\} + g^{\nu_\ell\ell}\left(\bar{\ell}\gamma^\mu P_L \nu_\ell\right)\right]W_\mu'^+ + \text{ h.c.}, \quad (2.14)$$

where g is the SM Weak coupling, V_{ij} represents the relevant CKM matrix element, g_X^{ij} $(X = L, R)$ and $g^{\nu_\ell\ell}$ are the NP couplings of the W' boson with the SM quarks and leptons. Using the definition of the fermi constant, $G_F/\sqrt{2} = g^2/8m_W^2$, and integrating out the W' leads to the following effective Hamiltonian.

$$\mathcal{H}_{\text{eff}} = \frac{4G_F V_{cq}}{\sqrt{2}}\left[\bar{c}_i\gamma^\mu\left(\frac{M_W^2}{M_{W'}^2}g_L^{cq}P_L + \frac{M_W^2}{M_{W'}^2}g_R^{cq}P_R\right)q\right]\left[g^{\nu_\ell\ell}\bar{\ell}\gamma_\mu P_L \nu_\ell\right] + \text{ h.c.} \quad (2.15)$$

Comparing Eq. (2.15) with Eq. (2.4) we obtain the following relations:

$$V_L = \frac{M_W^2}{M_{W'}^2}g_L^{cq}\sum_{\nu_\ell}g^{\nu_\ell\ell}, \qquad V_R = \frac{M_W^2}{M_{W'}^2}g_R^{cq}\sum_{\nu_\ell}g^{\nu_\ell\ell}. \quad (2.16)$$

3 Flavor Observables

In this section, we discuss the low-energy fits to the WCs of the effective Lagrangian from low-energy data and select a few benchmarks for NP. There are two main types of observables, listed below, that we are interested in for benchmarking.

- **Two-body decays:** $D_s^+ \to \ell^+\nu$, $D^+ \to \ell^+\nu$

- **Three-body decays:** $D \to K\ell\nu$, $D \to \pi\ell\nu$, $D \to K^*\ell\nu$, $D \to \rho\ell^+\nu$, $D_s^+ \to \phi\ell^+\nu$, $D_s^+ \to \eta^{(\prime)\ell\nu}$, $\Lambda_c \to \Lambda\ell\nu$

In the following sections, we will discuss benchmarks obtained from the above list. In our analysis we will not include the weak decays of the vector mesons as they decay dominantly by the strong and electromagnetic interactions. Further we will ignore the tensor current contributions to the pseudoscalar charmed mesons and charmed baryon decays as the relevant form factors are not known very well.

3.1 Two-body meson decays

The decay rate for the process $M_{ij}^+ \to \ell^+\nu$, where M_{ij}^+ represents a pseudoscalar $q_u^i \bar{q}_d^j$ meson, can be expressed in the basis of Eq. (2.4) as [31] :

$$\Gamma_{M_{ij}^+ \to \ell^+\nu} \;=\; \frac{G_F^2 m_M m_\ell^2}{8\pi} |V_{ij}|^2 f_M^2 \left(1 - \frac{m_\ell^2}{m_M^2}\right)^2 \left\{ |1 + V_L - V_R|^2 + \frac{|S_L - S_R|^2 m_M^4}{m_\ell^2 (m_i + m_j)^2} \right\}, \quad (3.1)$$

where m_i is the mass of the $q_{u,d}^i$, V_{ij} represents the relevant CKM matrix element, and other symbols carry their usual meaning. All numerical inputs are listed in Table 7 in Appendix C. The SM predictions using these parameters are given in Table 1.

3.2 Three-body meson decays

The decay rate of the semileptonic three body meson decays $M_i \to M_j \ell\nu$ in the basis of the Hamiltonian in Eq. (2.4) can be written as [34, 35]:

$$\frac{d\Gamma}{dq^2} \;=\; \frac{G_F^2 |V_{ij}|^2}{192\pi^3 m_{M_i}^3} q^2 \sqrt{\lambda(m_{M_i}^2, m_{M_j}^2, q^2)} \left(1 - \frac{m_\ell^2}{q^2}\right)^2 \times$$
$$\left\{ |1 + V_L + V_R|^2 \left[\left(1 + \frac{m_\ell^2}{2q^2}\right) h_{V,0}^2(q^2) + \frac{3}{2}\frac{m_\ell^2}{q^2} h_{V,t}^2(q^2) \right] + \frac{3}{2}|S_L + S_R|^2 h_S^2(q^2) \right.$$
$$\left. + 3\mathcal{R}e\left[(1 + V_L + V_R)(S_L^* + S_R^*)\right] \frac{m_\ell}{\sqrt{q^2}} h_S(q^2) h_{V,t}(q^2) \right\}, \quad (3.2)$$

where $\lambda(x, y, z) = x^2 + y^2 + z^2 - 2(xy + yz + zx)$.

The semileptonic three-body decay rate for $M_i \to M_j^* \ell\nu$ decays is expressed as:

$$\frac{d\Gamma}{dq^2} \;=\; \frac{G_F^2 |V_{ij}|^2}{192\pi^3 m_{M_i}^3} q^2 \sqrt{\lambda(m_{M_i}^2, m_{M_j^*}^2, q^2)} \left(1 - \frac{m_\ell^2}{q^2}\right)^2 \times$$
$$\left\{ (|1 + V_L|^2 + |V_R|^2)\left(\left(1 + \frac{m_\ell^2}{2q^2}\right)(H_{V,+}^2(q^2) + H_{V,-}^2(q^2) + H_{V,0}^2(q^2)) + \frac{3}{2}\frac{m_\ell^2}{q^2} H_{V,t}^2 \right) \right.$$
$$-2\mathcal{R}e\left[(1 + V_L)V_R^*\right]\left(\left(1 + \frac{m_\ell^2}{2q^2}\right)(2H_{V,+}^2(q^2)H_{V,-}^2(q^2) + H_{V,0}^2(q^2)) + \frac{3}{2}\frac{m_\ell^2}{q^2} H_{V,t}^2(q^2) \right)$$
$$\left. +\frac{3}{2}|S_L - S_R|^2 H_S^2(q^2) + 3\mathcal{R}e\left[(1 + V_L - V_R)(S_L^* - S_R^*)\right]\frac{m_\ell}{\sqrt{q^2}} H_S(q^2) H_{V,t}(q^2) \right\}. \quad (3.3)$$

The above hadronic amplitudes in terms of the form factors are provided in Appendix B and the form factor parameters and other numerical inputs are detailed in Appendix C.

Decay	$\ell = e$		$\ell = \mu$		$\ell = \tau$	
	$\mathcal{B}^{\mathrm{SM}}$ (%)	$\mathcal{B}^{\mathrm{meas}}$ (%)	$\mathcal{B}^{\mathrm{SM}}$ (%)	$\mathcal{B}^{\mathrm{meas}}$ (%)	$\mathcal{B}^{\mathrm{SM}}$ (%)	$\mathcal{B}^{\mathrm{meas}}$ (%)
$D_s^+ \to \ell^+ \nu_\ell$	$(1.28 \pm 0.05) \times 10^{-5}$	$< 8.3 \times 10^{-3}$	0.546 ± 0.020	0.543 ± 0.015	5.32 ± 0.20	5.32 ± 0.11
$D^+ \to \ell^+ \nu_\ell$	$(8.85 \pm 0.47) \times 10^{-7}$	$< 8.8 \times 10^{-4}$	0.0376 ± 0.0020	0.0374 ± 0.0017	0.100 ± 0.005	0.120 ± 0.027
$D^+ \to \overline{K}^0 \ell^+ \nu_\ell$	8.99 ± 0.37	8.72 ± 0.09	8.77 ± 0.36	8.76 ± 0.19		
$D^0 \to K^- \ell^+ \nu_\ell$	3.54 ± 0.15	3.549 ± 0.026	3.45 ± 0.14	3.41 ± 0.04		
$D^+ \to \pi^0 \ell^+ \nu_\ell$	0.320 ± 0.031	0.372 ± 0.017	0.316 ± 0.030	0.350 ± 0.015		
$D^0 \to \pi^- \ell^+ \nu_\ell$	0.249 ± 0.024	0.291 ± 0.004	0.245 ± 0.023	0.267 ± 0.012		
$D^+ \to \overline{K}^*(892)^0 \ell^+ \nu_\ell$	5.84 ± 1.61	5.40 ± 0.10	5.52 ± 1.52	5.27 ± 0.15		
$D^0 \to K^*(892)^- \ell^+ \nu_\ell$	2.30 ± 0.64	2.15 ± 0.16	2.18 ± 0.60	1.89 ± 0.24		
$D^+ \to \rho^0 \ell^+ \nu_\ell$	0.212 ± 0.048	0.19 ± 0.01	0.203 ± 0.046	0.24 ± 0.04		
$D^0 \to \rho^- \ell^+ \nu_\ell$	0.171 ± 0.039	0.150 ± 0.012	0.163 ± 0.037	0.135 ± 0.013		
$D_s^+ \to \phi \ell^+ \nu_\ell$	2.68 ± 0.26	2.39 ± 0.16	2.53 ± 0.23	1.9 ± 0.5		
$D_s^+ \to \eta \ell^+ \nu_\ell$	2.96 ± 0.45	2.26 ± 0.05	2.91 ± 0.45	2.4 ± 0.5		
$D_s^+ \to \eta'(958) \ell^+ \nu_\ell$	0.909 ± 0.41	0.8 ± 0.04	0.869 ± 0.41	1.1 ± 0.5		
$\Lambda_c^+ \to \Lambda \ell^+ \nu_\ell$	3.92 ± 0.63	3.56 ± 0.13	3.80 ± 0.60	3.48 ± 0.17		

Table 1. List of observables used to constrain the new physics coefficients along with their SM predictions and measured branching fractions. The measured values are taken from the PDG [38] while the SM predictions are computed using the form factors defined in Appendix C and the CKM matrix elements listed in Table 7.

3.3 Three-body baryonic decays

In this work we also consider the semileptonic decay of charmed baryon $\Lambda_c \to \Lambda \ell \nu$. The decay rate in terms of new physics Wilson coefficients as defined in Eq. (2.4) has been adopted from Ref. [36, 37] for the $\Lambda_b \to \Lambda_c \ell \nu$ decay as :

$$\frac{d\Gamma}{dq^2} = \frac{G_F^2 |V_{cs}|^2 q^2}{384 \pi^3 m_{\Lambda_c}^3} \sqrt{Q_+ Q_-} \left(1 - \frac{m_\ell^2}{q^2}\right)^2 \left(A_1^{VA} + \frac{m_\ell^2}{2q^2} A_2^{VA} + \frac{3}{2} A_3^{SP} + \frac{3m_\ell}{\sqrt{q^2}} A_5^{VA-SP}\right),$$
(3.4)

where $Q_\pm = (m_{\Lambda_c} \pm m_\Lambda)^2 - q^2$ and the amplitudes A_i^X in terms of the form factors and WCs can be found in Ref. [37].

3.4 Low energy fit results

We fit the new physics Wilson coefficients in Eq. (2.4) to the observables listed in Table 1 separately for the electron and muon modes. In Table 1, we list the SM expectation and the measured values of the branching fractions for each decay mode. For our numerical analysis, we take the values of D-meson decay constants and lattice determinations of relevant CKM matrix elements from the FLAG Review [39] [1]. In Appendix C we list the relevant numerical inputs and form factors used in this article. Note that there are 12 measurements for the electron modes and 14 for the muon modes which are utilized to fit to the respective flavour specific Wilson coefficients. For the tau mode, however, we only have measurements for the two body leptonic decay of the $D_{(s)}$ meson. Furthermore, since the ν_τ detection efficiency at SND is low compared to the other lepton flavour, it is challenging to obtain any meaningful constraint on the new physics parameters. Hence, we do not fit to tau measurements in our analysis.

---

[1]Ref. [40] points out that the inclusion of a universal electroweak correction in the Wilson coefficient ϵ_L leads to a $\sim 1\%$ increase in ϵ_L. This also leads to a smaller value of $|V_{cs}|$ compared to the one obtained by the PDG [38]. In this work, however, we use $\epsilon_L = 1$ and $|V_{cs}|$ as given in the FLAG Review [39].

Model	Fit Parameters	χ^2/dof	Re$[\epsilon_L]$	Im$[\epsilon_L]$	Re$[\epsilon_R]$	Im$[\epsilon_R]$	Re$[\epsilon_S]$	Im$[\epsilon_S]$	Re$[\epsilon_P]$	Im$[\epsilon_P]$	pull
1	Re$[\epsilon_L]$, Im$[\epsilon_L]$, Re$[\epsilon_R]$, Im$[\epsilon_R]$, Re$[\epsilon_S]$, Im$[\epsilon_S]$, Re$[\epsilon_P]$, Im$[\epsilon_P]$	1.18/4	$-1.14(13)$	$-0.54(14)$	$-0.56(13)$	$0.32(14)$	$-0.53(14)$	$-0.17(40)$	$0.0(1.2)$	$0.0(1.2)$	2.95
2	Re$[\epsilon_L]$, Re$[\epsilon_R]$, Re$[\epsilon_S]$, Re$[\epsilon_P]$	1.36/8	$-0.877(60)$	–	$-0.83(7)$	–	$0.58(10)$	–	$0.0(1.2)$	–	2.92
3	Re$[\epsilon_L]$, Im$[\epsilon_L]$	9.8/10	$-0.0043(35)$	$0.014(25)$	–	–	–	–	–	–	0.32
4	Re$[\epsilon_L]$	9.8/11	$-0.0042(130)$	–	–	–	–	–	–	–	0.32
5	Re$[\epsilon_R]$, Im$[\epsilon_R]$	9.7/10	–	–	$0.006(13)$	$0.00(13)$	–	–	–	–	0.45
6	Re$[\epsilon_R]$	9.7/11	–	–	$0.006(13)$	–	–	–	–	–	0.45
7	Re$[\epsilon_L]$, Im$[\epsilon_L]$, Re$[\epsilon_R]$, Im$[\epsilon_R]$	8.2/8	$-0.32(12)$	$-0.70(19)$	$0.021(90)$	$-0.21(26)$	–	–	–	–	1.3
8	Re$[\epsilon_L]$, Re$[\epsilon_R]$	8.2/10	$-0.028(24)$	–	$0.03(2)$	–	–	–	–	–	1.3
9	Re$[\epsilon_S]$, Im$[\epsilon_S]$	8.15/5	–	–	–	–	$-0.098(230)$	$0.0(9)$	–	–	0.52
10	Re$[\epsilon_S]$	8.15/6	–	–	–	–	$-0.098(230)$	–	–	–	0.52
11	Re$[\epsilon_P]$, Im$[\epsilon_P]$	1.79/4	–	–	–	–	–	–	$0.0(6)$	$0.0(6)$	0.004
12	Re$[\epsilon_P]$	1.79/5	–	–	–	–	–	–	$0.0(6)$	–	0.004
13	Re$[\epsilon_S]$, Im$[\epsilon_S]$, Re$[\epsilon_P]$, Im$[\epsilon_P]$	9.63/8	–	–	–	–	$-0.098(290)$	$0.0(8)$	$-0.002(600)$	$0.0(6)$	0.52
14	Re$[\epsilon_S]$, Re$[\epsilon_P]$	9.63/10	–	–	–	–	$-0.098(290)$	–	$-0.002(600)$	–	0.52
15	Re$[\epsilon_L]$, Im$[\epsilon_L]$, Re$[\epsilon_R]$, Im$[\epsilon_R]$, Re$[\epsilon_S]$, Im$[\epsilon_S]$	1.18/6	$-0.73(60)$	$-0.49(17)$	$0.46(60)$	$0.45(18)$	$0.56(34)$	$-0.032(180)$	–	–	2.95
16	Re$[\epsilon_L]$, Re$[\epsilon_R]$, Re$[\epsilon_S]$	1.35/8	$-0.88(6)$	–	$-0.83(7)$	–	$-0.58(11)$	–	–	–	2.92
17	Re$[\epsilon_L]$, Im$[\epsilon_L]$, Re$[\epsilon_R]$, Im$[\epsilon_R]$, Re$[\epsilon_P]$, Im$[\epsilon_P]$	8.2/6	$-0.54(14)$	$0.86(18)$	$0.014(130)$	$0.026(180)$	–	–	$0.0(4)$	$0.0(3)$	1.3
18	Re$[\epsilon_L]$, Re$[\epsilon_R]$, Re$[\epsilon_P]$	8.2/9	$-0.028(23)$	–	$0.030(24)$	–	–	–	$0.0(4)$	–	1.3

Table 2. Fit results for different combinations of WCs in decays to electrons. The SM chi-square for the full set of observables listed in Table 1 is $\chi^2_{SM}/dof = 9.90/12$ while for those affecting the scalar coupling only, $\chi^2_{SM,S}/dof = 8.43/7$, and correspondingly for the pseudoscalar coupling, $\chi^2_{SM,P}/dof = 1.79/6$.

The allowed parameter values for a specific model X corresponding to a specific lepton flavour is determined using

$$\chi^2(X) = \sum_{i=1}^{n} \frac{(\mathcal{B}_i^{\text{th}}(X) - \mathcal{B}_i^{\text{meas}})^2}{\sigma_i^2}, \tag{3.5}$$

where n is the total number of observables, $\mathcal{B}^{\text{th}}$ is the theoretical branching fraction, $\mathcal{B}^{\text{meas}}$ is the corresponding experimental measurement and σ is the uncertainty from measurement and theory added in quadrature. For a given model, the set of Wilson coefficients that minimize the above χ^2 function are found with their respective 1σ uncertainties using the algorithm supplied by the MINUIT package [41, 42] as shown in Tables 2, 3. We fit to both real and imaginary components of the Wilson coefficients denoted as $\epsilon_X = \text{Re}[\epsilon_X] + i\,\text{Im}[\epsilon_X]$ where X can be L, R, S, P. In each case, we define the pull with respect to the SM as $\sqrt{\chi^2(SM) - \chi^2(X)}$.

Note that, while all observables considered in this work are sensitive to vector-type new physics, not all decay rates are affected by the scalar coupling ϵ_S or pseudoscalar coupling ϵ_P. The two body leptonic decay of pseudoscalar mesons $M_i \to \ell\nu$ are purely sensitive to ϵ_P while that for the vector mesons are sensitive to neither ϵ_S nor ϵ_P. The three body semileptonic decays of the form $M_i \to M_j\ell\nu$ are affected by ϵ_S only while $M_i \to M_j^*\ell\nu$ rates are sensitive to ϵ_P only. The charmed baryonic decay $\Lambda_c \to \Lambda\ell\nu$, however, are influenced by both scalar and pseudoscalar new physics. Hence, while performing the fits to models

Model	Fit Parameters	χ^2/dof	Re$[\epsilon_L]$	Im$[\epsilon_L]$	Re$[\epsilon_R]$	Im$[\epsilon_R]$	Re$[\epsilon_S]$	Im$[\epsilon_S]$	Re$[\epsilon_P]$	Im$[\epsilon_P]$	pull
1	Re$[\epsilon_L]$, Im$[\epsilon_L]$, Re$[\epsilon_R]$, Im$[\epsilon_R]$, Re$[\epsilon_S]$, Im$[\epsilon_S]$, Re$[\epsilon_P]$, Im$[\epsilon_P]$	2.08/6	−1.71(10)	0.36(14)	−0.14(9)	−0.39(14)	−0.36(13)	−0.011(8)	0.007(8)	−0.009(7)	1.69
2	Re$[\epsilon_L]$, Re$[\epsilon_R]$, Re$[\epsilon_S]$, Re$[\epsilon_P]$	2.14/10	−0.097(10)	–	−0.049(14)	–	0.35(16)	–	−0.011(9)	–	1.67
3	Re$[\epsilon_L]$, Im$[\epsilon_L]$	4.87/12	−1.98(1.10)	−0.18(1.70)	–	–	–	–	–	–	0.26
4	Re$[\epsilon_L]$	4.87/13	−2.00(18)	–	–	–	–	–	–	–	0.26
5	Re$[\epsilon_R]$, Im$[\epsilon_R]$	4.83/12	–	–	0.0038(110)	0.0(2)	–	–	–	–	0.34
6	Re$[\epsilon_R]$	4.83/12	–	–	0.0038(110)	–	–	–	–	–	0.34
7	Re$[\epsilon_L]$, Im$[\epsilon_L]$, Re$[\epsilon_R]$, Im$[\epsilon_R]$	4.70/10	−1.91(28)	−0.41(15)	0.00(28)	0.00(15)	–	–	–	–	0.48
8	Re$[\epsilon_L]$, Re$[\epsilon_R]$	4.70/12	−0.004(12)	–	0.005(12)	–	–	–	–	–	0.48
9	Re$[\epsilon_S]$, Im$[\epsilon_S]$	1.24/5	–	–	–	–	−0.31(6)	0.00(34)	–	–	1.12
10	Re$[\epsilon_S]$	1.24/6	–	–	–	–	−0.31(6)	–	–	–	1.12
11	Re$[\epsilon_P]$, Im$[\epsilon_P]$	2.70/6	–	–	–	–	–	–	−0.00014(13)	0.00000(13)	0.01
12	Re$[\epsilon_P]$	2.70/7	–	–	–	–	–	–	−0.00014(13)	–	0.01
13	Re$[\epsilon_S]$, Im$[\epsilon_S]$, Re$[\epsilon_P]$, Im$[\epsilon_P]$	3.68/10	–	–	–	–	−0.31(16)	0.00(33)	−0.00013(13)	0.00000(13)	1.12
14	Re$[\epsilon_S]$, Re$[\epsilon_P]$	3.68/12	–	–	–	–	−0.31(16)	–	−0.00013(13)	–	1.12
15	Re$[\epsilon_L]$, Im$[\epsilon_L]$, Re$[\epsilon_R]$, Im$[\epsilon_R]$, Re$[\epsilon_S]$, Im$[\epsilon_S]$	2.65/8	−0.11(26)	0.09(15)	−0.057(80)	−0.19(27)	0.36(31)	−0.04(40)	–	–	1.51
16	Re$[\epsilon_L]$, Re$[\epsilon_R]$, Re$[\epsilon_S]$	2.65/10	−0.082(40)	–	−0.075(40)	–	0.36(15)	–	–	–	1.51
17	Re$[\epsilon_L]$, Im$[\epsilon_L]$, Re$[\epsilon_R]$, Im$[\epsilon_R]$, Re$[\epsilon_P]$, Im$[\epsilon_P]$	3.76/8	−0.51(10)	−0.83(32)	0.016(100)	−0.028(320)			−0.007(400)	0.011(22)	1.09
18	Re$[\epsilon_L]$, Re$[\epsilon_R]$, Re$[\epsilon_P]$	3.76/10	−0.031(30)	–	0.033(30)	–	–	–	−0.013(6)	–	1.09

Table 3. Similar to Table 2, but for the muon observables with $\chi^2_{SM}/dof = 4.94/14$, $\chi^2_{SM,S}/dof = 2.5/7$ and $\chi^2_{SM,P}/dof = 2.7/8$.

involving either ϵ_S or ϵ_P only, we drop the decay modes that are redundant to the analysis for that particular coupling. The SM chi-squares are calculated accordingly in order to estimate the pull with respect to new physics. As mentioned in the caption of Table 2, the SM chi-square value per degree of freedom (dof) for the full set of 12 observables listed in Table 1 is calculated to be $\chi^2_{SM}/dof = 9.9/12$ while, for the observables sensitive to ϵ_S only, $\chi^2_{SM,S}/dof = 8.43/7$, and, for those affected by ϵ_P, $\chi^2_{SM,P}/dof = 1.79/6$. Similarly, for the muon fit, the respective SM chi-squares are found to be $\chi^2_{SM}/dof = 4.94/14$, $\chi^2_{SM,S}/dof = 2.5/7$ and $\chi^2_{SM,P}/dof = 2.7/8$.

The pseudoscalar coupling ϵ_P is tightly constrained from the two body decays $D_s^+ \to \ell^+ \nu_\ell$ and $D^+ \to \ell^+ \nu_\ell$. However, the lack of measurement of these decay rates for the electron channel keeps ϵ_P practically unconstrained as is reflected in the fit results in Table 2. In case of the muon, ϵ_P is better constrained due to the availability of the measurements of the two body decays and we obtained tightly constrained central values with small error bars as shown in Table 3. For the scalar and vector couplings, there is an interplay between the semileptonic mesonic three body decays and the charmed baryon decays resulting in very small to even $\mathcal{O}(1)$ central values for the real and imaginary parts of the parameters.

4   Deep Inelastic Neutrino-Nucleon Scattering

In this section, we explore the sensitivity of SND@LHC to NP, as encapsulated in the WCs defined in Eq. (2.4). Given the high energy of the incoming neutrinos, neutrino detection

proceeds through charged-current deep-inelastic scattering (DIS):

$$\nu_\ell + N \to \ell + X, \tag{4.1}$$

where $N = p, n$ represents a nucleon, $\ell = e, \mu, \tau$ and X denotes any hadron state. However, NP contributes specifically to charm production, as shown in Fig. 1:

$$\nu_\ell + N \to \ell + X_c, \tag{4.2}$$

where X_c denotes a possible charm hadron state. In this analysis, we evaluate the confidence level with which the WCs obtained by fitting low-energy observables, as summarized in Tables 2 and 3, can be probed at SND@LHC.

The sensitivity is determined through a χ^2 analysis for each type of neutrino using the following definition:

$$\chi^2 = \sum_{i=1}^{n} \left(\frac{N_i^{\text{SM+NP}} - N_i^{\text{SM}}}{\sqrt{N_i^{\text{SM+NP}}}} \right)^2, \tag{4.3}$$

where N_i^{SM} are the number of differential events predicted by the SM and $N_i^{\text{SM+NP}}$ are the total number of differential events, including contributions from NP, for the ith bin in the energy distribution.

We also assess the sensitivity to NP in the ratio,

$$R_{\mu e,i} \equiv \frac{N_{\mu,i}}{N_{e,i}}, \tag{4.4}$$

for WCs provided in Tables 2 and 3, considering scenarios where NP effects are exclusively present in either muons or electrons. Here, $N_{\mu(e),i}$ represents the model prediction of the number of events for the process $\nu_\ell + N \to \ell + X/X_c$ in the i-th energy bin. We then define the χ^2 for this observable as

$$\chi^2 = \sum_{i=1}^{n} \left(\frac{R_{\mu e,i}^{\text{SM + NP}} - R_{\mu e,i}^{\text{SM}}}{\sigma_{R_{\mu e,i}^{\text{SM + NP}}}} \right)^2, \tag{4.5}$$

where $\sigma_{R_{\mu e,i}^{\text{SM+NP}}}$ is the statistical error in $R_{\mu e,i}$ and is calculated as follows.

$$\sigma_{R_{\mu e,i}}^2 \equiv R_{\mu e,i}^2 \left(\frac{\sigma_{e,i}^2}{N_{e,i}^2} + \frac{\sigma_{\mu,i}^2}{N_{\mu,i}^2} \right) = R_{\mu e,i}^2 \left(\frac{1}{N_{e,i}} + \frac{1}{N_{\mu,i}} \right), \tag{4.6}$$

where in the final step we have assumed that the event distribution follows Poisson statistics so that $\sigma_{\mu(e),i}^2 = N_{\mu(e),i}$.

For signal or background, the total number of events is calculated from the DIS cross-section, $\sigma_{\nu N}$, as follows:

$$N_i^{\text{model}} = \mathcal{L} \times \sigma(pp \to \nu X) \times A_g \times P_{\text{int}}(\sigma_{\nu N}^{\text{model}}), \tag{4.7}$$

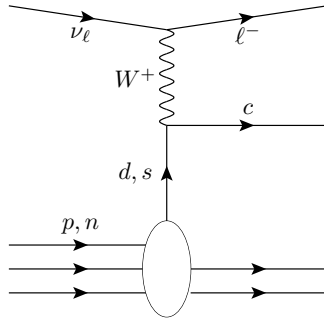$$= \Phi_{i,\nu} \times P_{\text{int}}(\sigma_{\nu N}^{\text{model}}) \tag{4.8}$$

Figure 1. Feynman diagram illustrating charged-current deep-inelastic scattering. This diagram with reversed arrows also applies to anti-neutrino interactions where an anti-strange quark ($\bar{s}$) is picked from the nucleon.
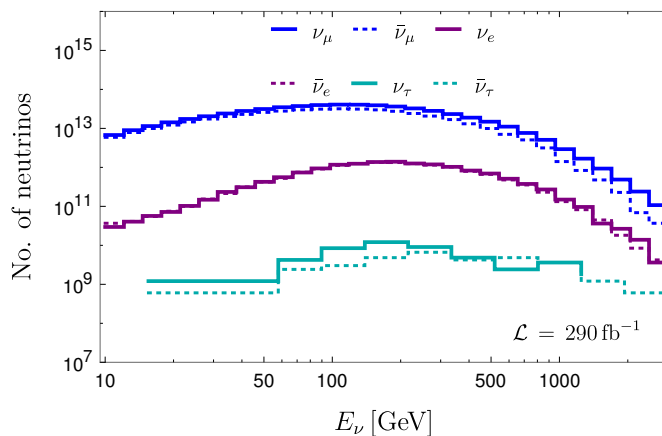

Figure 2. Number of incoming neutrinos in SND@LHC as a function of energy. The spectrum is obtained from Ref. [30], scaling to an expected integrated luminosity of $\mathcal{L} = 290$ fb^{-1} and selecting only the neutrinos within the SND@LHC geometrical acceptance.

where $\mathcal{L} = 290$ fb^{-1} is the pp luminosity, $\sigma(pp \to \nu X)$ is the cross-section for neutrino production in pp collisions, A_g is the geometrical acceptance of SND@LHC, and the product of these factors constitutes the incoming neutrino spectra $\Phi_{i,\nu}$ in the ith energy bin. $P_{\text{int}}(\sigma_{\nu N}^{\text{model}})$ represents the interaction probability of a neutrino with the detector, which is a function of the DIS cross-section. Here, model refers to background (SM) or signal (SM+NP).

We take and adapt the spectra of neutrinos produced at the ATLAS LHC interaction point and impinging onto the SND@LHC detector from Ref. [30]. These were obtained using the Pythia8, DPMJET and FLUKA library to simulate the production of neutrinos in pp collisions, and their propagation through the machine elements until the location of the SND@LHC target. Only neutrinos within the SND@LHC geometrical acceptance A_g are retained. These spectra are scaled up to an expected luminosity of $\mathcal{L} = 290$ fb^{-1} and shown in Fig. 2.

To this end, the interaction probability of a neutrino with the detector is computed

as:

$$P_{\text{int}} = \frac{A \, \sigma_{\nu N}^{\text{model}}}{\mathcal{S}} \frac{m_{\text{target}}}{m_{\text{N}}} \tag{4.9}$$

where $\sigma_{\nu N}^{\text{model}}$ is the charge current scattering cross-section for Eqs. (4.1), (4.2). The detector consists of 5 walls, each with 2×2 tungsten bricks with an area perpendicular to the beam direction of $\mathcal{S} = 400 \times 400 \, \text{mm}^2$ [30]. The total mass of the detector is $m_{\text{target}} = 830$ kg [30], and $m_{\text{N}} = 3.05 \times 10^{-25}$ kg is the mass of a tungsten nucleus. The length of the detector is $l_{\text{target}} = 59 \times 5$ mm, and the mass number of tungsten is A=183.

The cross-section $\sigma_{\nu N}$ is obtained as follows.

The differential cross-section for an incoming neutrino with energy E_ν scattering off a nucleon of mass M in terms of the scattering amplitude is:

$$\frac{d\sigma_{\nu N}}{dxdy} = \frac{1}{32\pi M E_\nu} \int \frac{d\xi}{\xi} f(\xi) |\bar{\mathcal{M}}(\xi)|^2 \delta(\xi - x). \tag{4.10}$$

where ξ is the momentum fraction defined by $p_q^\mu = \xi p^\mu$, with p_q^μ being the four-momentum of the scattered quark and p^μ the target nucleon momentum. The function $f(\xi)$ represents the parton distribution function (PDF) within the nucleon. We further decompose the differential cross-section of the neutrino-nucleon DIS into contributions from the SM, NP operators, and their interference terms:

$$\frac{d\sigma_{\nu N}^{\text{SM+NP}}}{dxdy} = \frac{d\sigma_{\nu N}^{\text{SM}}}{dxdy} + \frac{d\sigma_{\nu N}^{\text{NP}}}{dxdy} + \frac{d\sigma_{\nu N}^{\text{Interference}}}{dxdy}, \tag{4.11}$$

where x is the Bjorken variable and y is the inelasticity with q being the four-momentum transfer of the leptonic probe and $\nu = -p \cdot q = M(E_\nu - E_\ell)$. The complete expressions for these terms are provided below for different interactions.

Scalar interactions: Using Ref. [26], we have

$$\frac{d\sigma_{\nu N}^{\text{SM}}}{dxdy} = \frac{G_F^2 M E_\nu}{\pi} \left(xy^2 + \frac{ym_\ell^2}{2ME_\nu} \right)F_1 + \left(1 - y - \frac{Mxy}{2E_\nu} - \frac{m_\ell^2}{4E_\nu^2}\right)F_2$$
$$+ \left(xy - \frac{xy^2}{2} - \frac{ym_\ell^2}{4ME_\nu}\right)F_3 - \frac{m_\ell^2}{2ME_\nu}F_5 \bigg),$$
$$\frac{d\sigma_{\nu N}^{\text{S}}}{dxdy} = \frac{G_F^2 M E_\nu}{\pi}(\epsilon_S^2 + \epsilon_P^2)y\left(xy + \frac{m_\ell^2}{2ME_\nu}\right)F_1,$$
$$\frac{d\sigma_{\nu N}^{\text{SM,S}}}{dxdy} = 0. \tag{4.12}$$

The functions F_i are given as

$$F_1 = \sum_{q,\bar{q}} f_{q,\bar{q}}(\xi, Q^2)V_{q,c}^2,$$
$$F_2 = 2\sum_{q,\bar{q}} \xi f_{q,\bar{q}}(\xi, Q^2)V_{q,c}^2,$$
$$F_3 = 2\sum_q f_q(\xi, Q^2)V_{q,c}^2 - 2\sum_{\bar{q}} f_{\bar{q}}(\xi, Q^2)V_{\bar{q},\bar{c}}^2,$$
$$F_5 = 2\sum_{q,\bar{q}} f_{q,\bar{q}}(\xi, Q^2)V_{q,c}^2, \tag{4.13}$$

where f_q and $f_{\bar{q}}$ are the parton distribution functions inside a nucleon, $V_{q,q'}$ is the CKM matrix element, and $Q^2 = -q^2$.

Vector and axial vector interactions: For vector and axial interactions, we have

$$
\begin{aligned}
\frac{d\sigma_{\nu N}^{\text{SM+VA}}}{dxdy} =\ & \frac{G_F^2 M E_\nu}{\pi} \left[\left(\frac{|a'|^2 + |b'|^2}{2} \right) \left(\frac{y m_\ell^2}{2 M E_\nu} + xy^2 \right) F_1(x) \right. \\
& + \left(\frac{|a'|^2 + |b'|^2}{2} \right) \left(1 - y - \frac{xyM}{E_\nu} - \frac{m_\ell^2}{4 E_\nu^2} \right) F_2(x) \\
& \left. + \text{Re}(a'b'^*) \left(xy - \frac{xy^2}{2} - \frac{y m_l^2}{4 M E_\nu} \right) F_3(x) - \left(\frac{|a'|^2 + |b'|^2}{2} \right) \frac{m_l^2}{2 M E_\nu} F_5(x) \right]
\end{aligned}
\tag{4.14}
$$

where $a' = 1 + \epsilon_L + \epsilon_R$ and $b' = 1 + \epsilon_L - \epsilon_R$.

The total cross-section $\sigma_{\nu N}$ is obtained by integrating the differential cross-section over the following limits:

$$
\frac{m_l^2}{2M(E_\nu - m_l)} \leq x \leq 1,
\tag{4.15}
$$

$$
A - B \leq y \leq A + B
\tag{4.16}
$$

where

$$
A = \frac{1}{2} \left(1 - \frac{m_l^2}{2 M E_\nu x} - \frac{m_l^2}{2 E_\nu^2} \right) \Big/ \left(1 + \frac{xM}{2 E_\nu} \right),
\tag{4.17}
$$

$$
B = \frac{1}{2} \left[\left(1 - \frac{m_l^2}{2 M E_\nu x} \right)^2 - \frac{m_l^2}{E_\nu^2} \right] \Big/ \left(1 + \frac{xM}{2 E_\nu} \right).
\tag{4.18}
$$

5 Results

The SND@LHC detector covers the pseudorapidity range of $7.2 < \eta < 8.4$ [28]. We obtain event distributions as functions of the neutrino energy, E_ν, for both background (SM) and signal (SM + NP) events, by applying the appropriate pseudorapidity cuts. The NP scenarios we study are listed in Tables 2 and 3 and were obtained by fitting to low-energy observables. We then use the energy distributions to calculate the sensitivity to NP at SND@LHC, by applying Eq. (4.8) in conjunction with Eq. (4.3) and Eq. (4.5).

In principle, NP affecting charm quarks, as encoded in the effective Hamiltonian of Eq. (2.4), will also impact the production flux of neutrinos. Ref. [43] demonstrates that charm-hadron decays predominantly drive the electron-neutrino flux at energies above 200 GeV, while they contribute equally to the muon-neutrino flux, along with pion decays, at energies above 400 GeV. These effects have been thoroughly analyzed in Ref. [29] for all neutrino flavors. Their study shows that an NP pseudoscalar interaction with order-one coupling significantly amplifies the flux at production due to 2-body D_s decays, increasing the electron-neutrino flux by up to $10^3\times$ and the muon-neutrino flux by up to $27\times$ than in the SM. However, ν_e and ν_μ production are dominated by three-body D_s decays, which

unlike two-body D_s decays are not similarly enhanced. Therefore, these production and detection enhancements do not impact our analysis, as we only consider NP in the charm sector. We emphasize that, even if NP were present in first-generation quarks, stringent low-energy constraints impose strong limits on the corresponding Wilson coefficients, rendering current neutrino detectors ineffective in probing such NP operators. Furthermore, in our analysis even at a high luminosity, significant sensitivity to NP affecting muons is only observed when the final state is charm tagged. We, therefore, assume a 100% charm-tagging efficiency.
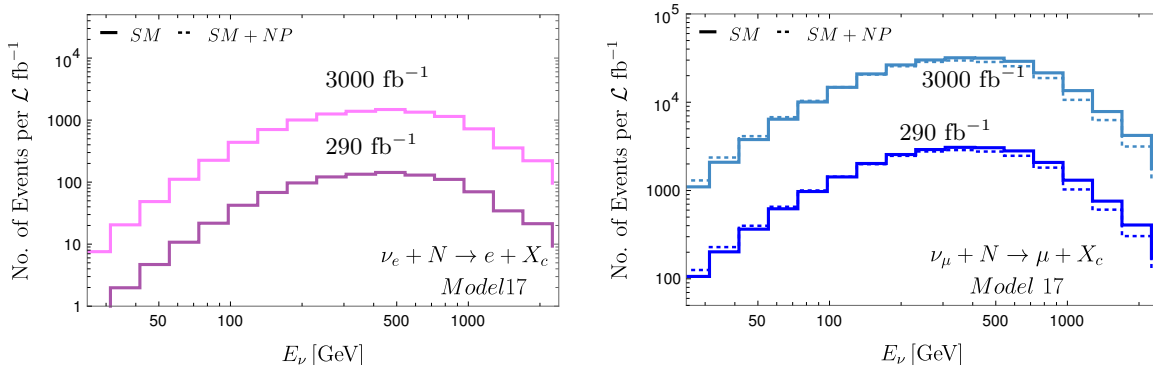
Figure 3. Number of signal (SM + NP, dashed) and background (SM only, solid) events as functions of the incoming neutrino energy (E_ν) for $\nu_e + N \to e^- + X_c$ (left plot) and $\nu_\mu + N \to \mu + X_c$ (right plot.) The integrated luminosity $\mathcal{L}$ has been set to the SND@LHC current projection of 290 fb^{-1} for the lower (dark blue/dark pink) histograms, and to its high-lumi upgrade projection of 3000 fb^{-1} for the upper (light blue/light pink) histograms. These results use couplings of model 17 from Tables 2 and 3, alongwith the pseudorapidity range $7.2 < \eta < 8.4$ corresponding to the SND@LHC detector.

The resulting event distributions for the electron and muon neutrinos are presented in Fig. 3. As can be seen in Fig. 3, the NP contribution is negligible for the electron neutrino. In Table 4, we present our results for the sensitivities of detecting NP with muons in the final state. This sensitivity is influenced by the left- and right-handed vector couplings. These results are based on the central values of NP couplings listed in Table 3. Here, we only include those cases where the sensitivity exceeds $0.1\,\sigma$. The high-luminosity upgrade

Models	Sens($\nu_\mu + N \to \mu + X_c$)	Sens$\left(\dfrac{\nu_\mu + N \to \mu + X_c}{\nu_{e^-} + N \to e^- + X_c} \right)$
1	0.3σ	0.1σ
17	0.4σ	0.1σ

Table 4. Sensitivity (Sens) of detecting NP in the signal $\nu_\mu + N \to \mu + X_c$ at SND@LHC for models in Table 3 where the significance exceeds 0.1σ. It also shows the sensitivity for finding NP in the ratio $\left(\frac{\nu_\mu + N \to \mu + X_c}{\nu_{e^-} + N \to e^- + X_c} \right)$, assuming NP is present only in the muon interaction (i.e., the numerator). The significances are calculated for a luminosity of 290 fb^{-1}.

of SND@LHC can collect ten times more data [44], significantly enhancing the sensitivity to NP, even in models where no significant sensitivity is observed at $\mathcal{L} = 290\,\mathrm{fb}^{-1}$. We

assess the sensitivity for a luminosity of 3000 fb^{-1} in Table 5. Fig. 3 also includes event distributions for the high-lumi upgrade of SND@LHC.

Models	Sens($\nu_\mu + N \to \mu + X_c$)	Sens$\left(\dfrac{\nu_\mu + N \to \mu + X_c}{\nu_{e^-} + N \to e^- + X_c} \right)$
1	2.8σ	1.2σ
2	0.5σ	0.1σ
17	3.1σ	1.4σ

Table 5. Sensitivity of detecting NP in the signal $\nu_\mu + N \to \mu + X_c$ at SND@LHC, based on models listed in Table 3, assuming a luminosity of 3000 fb^{-1}.

Finally, we note the importance of ν_τ scattering at experiments such as SND@LHC. NP effective operators involving both the charm quark and the τ neutrino are difficult to constrain from low-energy measurements. Due to the relative closeness in the τ and charm masses, three-body decays are suppressed or prohibited due to phase-space effects. In these cases, neutrino scattering experiments can shed a significant amount of light on such NP operators. In this article, however, we restrict ourselves to the cases where neutrino scattering experiments can provide information complementary to low-energy constraints, and as such do not consider τ-neutrino scattering.

6 Conclusion

In this paper, we have presented a detailed sensitivity analysis of new physics (NP) and lepton universality violation (LUV) in neutrino scattering at SND@LHC, focusing on processes involving a charm quark in the final state. Within the framework of effective field theory, NP effects were described using higher-dimensional four-Fermi operators. The Wilson coefficients for these dimension-6 operators were determined from fits to low-energy data, particularly from decays of charmed mesons and baryons. Using benchmark NP points derived from these low-energy analyses, we provide sensitivity estimates for detecting NP and LUV effects at SND@LHC. Both production and scattering processes of neutrinos were considered in evaluating NP effects.

Our study shows that SND@LHC exhibits significant sensitivity to these operators only when both charm tagging is effective and high luminosity is achieved, as NP couplings are tightly constrained by low-energy measurements. The inability of neutrino detectors to probe NP under these constraints aligns with the findings from FASERν, when their analyses of NP constraints and detector sensitivity are considered together [29]. However, effective charm tagging at high luminosity emerges as a key factor that could enhance the sensitivity to the 3σ level. In principle, the high-lumi upgrade of SND@LHC could gather 10 times more statistics [44], which will lead to higher sensitivities to NP effects in the ν_μ channel.

We also believe that a more comprehensive, multi-dimensional analysis could further improve the sensitivity. Additionally, our findings indicate that these detectors may be sensitive to NP operators that evade low-energy constraints but become relevant at high-energy scales. One such operator, as proposed in Ref. [45], fits this profile, though we

leave a detailed investigation for future work. Furthermore, since effective couplings involving charmed particle decays with a final state ν_τ receive less stringent constraints from low-energy experiments due to phase space restrictions, we note that neutrino scattering experiments can provide useful information about NP in such effective operators.

A Lepton Universality Violation in charged-current B decays

Table 6 below summarizes experimental measurements and SM predictions in several charged-current B decays. The $R_{D^{(*)}}^{\tau/\ell}$ values roughly show a 2.1-2.2 σ deviation from the SM. However, these measurements are correlated and the combined deviation from the SM appears to be around 3.2σ [1]. A 1.7σ deviation is currently observed in $R_{J/\psi}^{\tau/\mu}$. While there is no observed deviation from the SM, current measurements allow LUV at the 3-5% level in $R_{D^{(*)}}^{\mu/e}$. Together these observables provide strong hints of Lepton Universality Violating (LUV) new physics (NP) in charged-current B decays.

Observable	SM Prediction	Measurement
$R_{D^*}^{\tau/\ell}$	0.254 ± 0.005 [17]	0.287 ± 0.012 [17]
$R_D^{\tau/\ell}$	0.298 ± 0.004 [17]	0.342 ± 0.026 [17]
$R_{J/\psi}^{\tau/\mu}$	0.283 ± 0.048 [46]	$0.71 \pm 0.17 \pm 0.18$ [16]
$R_{D^*}^{\mu/e}$	~ 1.0	$1.04 \pm 0.05 \pm 0.01$ [47]

Table 6. Standard Model predictions and measured values of observables that may provide hints of LUV NP in charged-current B decays.

B Hadronic amplitudes for three body decays

The hadronic matrix element of the vector current for the three body decay $M_i \to M_j \ell\nu$ in terms of the form factors $f_{+,0}(q^2)$ is given as

$$\langle M_j(k')|\bar{q}_j\gamma_\mu c|M_i(k)\rangle = f_+(q^2)\left((k+k')_\mu - \frac{m_{M_i}^2 - m_{M_j}^2}{q^2}q_\mu\right) + f_0(q^2)\frac{m_{M_i}^2 - m_{M_j}^2}{q^2}q_\mu.$$
$$(B.1)$$

Using the equation of motion, $i\partial_\mu(\bar{q}_j\gamma^\mu c) = (m_c - m_j)(\bar{q}_j c)$, the scalar matrix element can be written as

$$\langle M_j|\bar{q}_j c|M_i\rangle = f_0(q^2)\frac{m_{M_i}^2 - m_{M_j}^2}{m_c - m_j}. \tag{B.2}$$

The non-vanishing helicity amplitudes in terms of the form factors are given by

$$h_{V,0}^2(q^2) = \sqrt{\frac{\lambda(m_{M_i}^2, m_{M_j}^2, q^2)}{q^2}}f_+(q^2), \tag{B.3}$$

$$h_{V,t}^2(q^2) = \frac{m_{M_i}^2 - m_{M_j}^2}{\sqrt{q^2}}f_0(q^2), \tag{B.4}$$

$$h_S^2(q^2) \simeq \frac{m_{M_i}^2 - m_{M_j}^2}{m_c - m_j}f_0(q^2). \tag{B.5}$$

Similarly, the vector and axial vector hadronic matrix elements for the $M_i \to M_j^*\ell\nu$ decays as a function of the form factors can be written as

$$\langle M^*(k,\varepsilon)|\bar{q}_j\gamma_\mu c|\overline{M}_i(p)\rangle = -i\epsilon_{\mu\nu\rho\sigma}\varepsilon^{\nu*}p^\rho k^\sigma\frac{2V(q^2)}{m_{M_i} + m_{M_j^*}}, \tag{B.6}$$

$$\langle M^*(k,\varepsilon)|\bar{q}_j\gamma_\mu\gamma_5 c|\overline{M}_i(p)\rangle = \varepsilon^{\mu*}(m_{M_i} + m_{M_{j*}})A_1(q^2) - (p+k)_\mu(\varepsilon^*q)\frac{A_2(q^2)}{m_{M_i} + m_{M_{j*}}}$$

$$- q_\mu(\varepsilon^*q)\frac{2m_{M_j^*}}{q^2}(A_3(q^2) - A_0(q^2)), \tag{B.7}$$

where

$$A_3(q^2) = \frac{m_{M_i} + m_{M_{j*}}}{2m_{M_j^*}}A_1(q^2) - \frac{m_{M_i} - m_{M_{j*}}}{2m_{M_j^*}}A_2(q^2). \tag{B.8}$$

The kinematic constraint at zero recoil gives $A_3(0) = A_0(0)$. The pseudoscalar matrix element is determined using the equation of motion $i\partial_\mu(\bar{q}_j\gamma^\mu\gamma^5 c) = -(m_c + m_j)(\bar{q}_j\gamma^5 c)$ and is given by

$$\langle M^*(k,\varepsilon)|\bar{q}_j\gamma_5 c|\overline{M}_i(p)\rangle = -(\varepsilon^*q)\frac{2m_{M_{j*}}}{m_c + m_j}A_0(q^2). \tag{B.9}$$

The helicity amplitudes in terms of the form factors are given as

$$H_{V,\pm}(q^2) = (m_{M_i} + m_{M_{j*}})A_1(q^2) \mp \frac{\sqrt{\lambda(m_{M_i}^2, m_{M_j^*}^2, q^2)}}{m_{M_i} + m_{M_j^*}}V(q^2), \tag{B.10}$$

$$H_{V,0}(q^2) = \frac{m_{M_i} + m_{M_{j*}}}{2m_{M_j^*}\sqrt{q^2}}\Bigg\{-(m_{M_i}^2 - m_{M_j^*}^2 - q^2)A_1(q^2)$$

$$+ \frac{\lambda(m_{M_i}^2, m_{M_j^*}^2, q^2)}{(m_{M_i} + m_{M_j^*})^2}A_2(q^2)\Bigg\}, \tag{B.11}$$

$$H_{V,t}(q^2) = -\sqrt{\frac{\lambda(m_{M_i}^2, m_{M_j^*}^2, q^2)}{q^2}}A_0(q^2), \tag{B.12}$$

$$H_S(q^2) \simeq -\frac{\sqrt{\lambda(m_{M_i}^2, m_{M_j^*}^2, q^2)}}{m_c + m_j}A_0(q^2). \tag{B.13}$$

As mentioned earlier, we incorporate the hadronic matrix elements for the baryonic $\Lambda_c \to \Lambda \ell \nu$ decays from Ref. [37].

C   Numerical inputs and form factors

Here we collect the relevant numerical inputs (in Table 7) and form factors for the charmed hadron decays to pions, kaons, and other light pseudoscalar and vector resonances used in the analysis.

G_F	1.166×10^{-5} [38]	m_{K^+}	493.677 MeV [38]
f_{D_s}	249.9(5) MeV [39]	m_{K^0}	497.611 MeV [38]
f_D	212.0(7) MeV [39]	m_{π^+}	139.57 MeV [38]
$|V_{cs}|$	0.983(2)(18) [39]	m_{π^0}	134.98 MeV [38]
$|V_{cd}|$	0.2179(7)(57) [39]	$m_{K^{*+}}$	891.67 MeV [38]
τ_{D_s}	0.501 ps [38]	$m_{K^{*0}}$	895.55 MeV [38]
τ_{D^+}	1.033 ps [38]	m_{ρ^+}	766.5 MeV [38]
τ_{D^0}	0.410 ps [38]	m_{ρ^0}	775.26 MeV [38]
$m_{D_s^+}$	1968.35 MeV [39]	m_ϕ	1.019 GeV [38]
m_{D^+}	1869.66 MeV [38]	m_η	547.86 MeV [38]
m_{D^0}	1864.84 MeV [38]	$m_{\eta'}$	957.78 Me [38]
m_{D^*}	2.1122 GeV [38]	m_{Λ_c}	2.286 GeV [38]
$m_{D^{*0}}$	2.317 GeV [38]	m_Λ	1.116 GeV [38]

Table 7. List of all numerical inputs used in the analysis.

For the $D \to \pi \ell \nu_\ell$ transition, the q^2 dependence of two relevant form factors $f_{+,0}^{D \to \pi}$ can be expressed as [48]:

$$f_+^{D \to \pi}(q^2) = \frac{1}{1 - P_V q^2}\left\{ f^{D \to \pi}(0) + c_+^{D \to \pi}(z - z_0)\left(1 + \frac{z + z_0}{2}\right) \right\}, \qquad (C.1)$$

$$f_0^{D \to \pi}(q^2) = \frac{1}{1 - P_S q^2}\left\{ f^{D \to \pi}(0) + c_0^{D \to \pi}(z - z_0)\left(1 + \frac{z + z_0}{2}\right) \right\}, \qquad (C.2)$$

where z is defined as

$$z = \frac{\sqrt{t_+ - q^2} - \sqrt{t_+ - t_0}}{\sqrt{t_+ - q^2} + \sqrt{t_+ - t_0}}, \qquad (C.3)$$

with

$$t_+ = (m_D + m_\pi)^2, \qquad (C.4)$$

$$t_0 = (m_D + m_\pi)(\sqrt{m_D} - \sqrt{m_\pi})^2. \qquad (C.5)$$

The other parameters that appear in the z-expansion of the form factors are collected below in Table 8.

$f^{D\to\pi}(0)$	$c_+^{D\to\pi}$	P_V (GeV^{-2})	$c_0^{D\to\pi}$	P_S (GeV^{-2})
0.6117(354)	-1.985(347)	0.1314(127)	-1.188(256)	0.0342(122)

Table 8. Values of the parameters taken from [48] that appear in the z-expansion of the vector and scalar form factors of the $D \to \pi$ transition.

A similar kind of z-expansion is also employed in case of the $D \to K$ transition are expressed as

$$f_+^{D\to K}(q^2) = \frac{1}{1-q^2/m_{D^*}^2}\left(a_0^+ + a_1^+(z - z^3/3) + a_2^+(z^2 + 2z^3/3)\right), \tag{C.6}$$

$$f_0^{D\to K}(q^2) = \frac{1}{1-q^2/m_{D^{*0}}^2}\left(a_0^0 + a_1^0\, z + a_2^0\, z^2)\right), \tag{C.7}$$

with $m_\pi \leftrightarrow m_K$ in Eqs. (C.4)-(C.5). The kinematic constraint at zero recoil $f_+^{D\to K}(0) = f_0^{D\to K}(0)$ reduces one parameter out of the six while rest of the coefficients are taken from the most recent FLAG $N_f = 2+1+1$ computation of the form factors [39] as listed in Table 9.

a_0^+	a_1^+	a_2^+	a_0^0	a_1^0
0.7877(87)	-0.97(18)	-0.3(2.0)	0.6959(47)	0.775(69)

Table 9. Values of form factor parameters relevant to the $D \to K$ transition as obtained by [39].

The form factors for the $D_s \to (\eta, \eta')\ell\nu$ transition are calculated based on the light cone QCD sum rules (LCSR) as in Ref. [49]. The q^2 dependence of the vector form factors is given by the form

$$f_\pm^{D_s\to\eta}(q^2) = \frac{f_\pm(0)^{D_s\to\eta}}{1 - \alpha_\pm\hat{q} + \beta_\pm\hat{q}^2}, \tag{C.8}$$

with $\hat{q} = q^2/m_{D_s}^2$ and the parameters $\alpha_\pm$, $\beta_\pm$ and $f_\pm(0)^{D_s\to\eta}$ are listed in Table. 10. The scalar form factor $f_0^{D_s\to\eta}$ is related to the vector ones by the relation

$$f_0^{D_s\to\eta}(q^2) = f_+^{D_s\to\eta}(q^2) + \frac{q^2}{m_{D_s}^2 - m_\eta^2}f_-^{D_s\to\eta}(q^2). \tag{C.9}$$

The form factors $f_i^{D_s\to\eta'}$ are related to $f_i^{D_s\to\eta}$ as [49]

$$\frac{|f_i^{D_s\to\eta}|}{|f_i^{D_s\to\eta'}|} = \tan\varphi, \tag{C.10}$$

where $\varphi = (39.7 \pm 0.7)°$ [49] is the mixing angle between the η and η' states.

A simple single pole parametrization is employed to calculate the form factors for the pseudoscalar $P = D, D_s$ to vector $M = K^*, \phi, \rho$ meson transitions given as

$$F_i^M(q^2) = \frac{F_i^M(0)}{1 - q^2/m_{R,i}^2}, \tag{C.11}$$

$f_+^{D_s\to\eta}(0)$	α_+	β_+	$f_-^{D_s\to\eta}(0)$	α_-	β_-
0.45(14)	1.96(63)	1.12(36)	-0.44(13)	2.05(65)	1.08(35)

Table 10. Values of form factor parameters relevant to the $D_s \to \eta$ transition as obtained by the LCSR calculation in Ref. [49].

F_i	K^* [50]		ρ [51]		ϕ [52]	
	$F_i(0)$	$m_{R,i}$ (GeV)	$F_i(0)$	$m_{R,i}$ (GeV)	$F_i(0)$	$m_{R,i}$ (GeV)
A_1	0.620(85)	2.459	$0.58^{+0.065}_{-0.050}$	2.427	0.615(24)	2.459
A_2	$r_2 A_1(0)$ $r_2 = 0.801(30)$	2.459	$0.468^{+0.052}_{-0.053}$	2.427	0.457(78)	2.459
V	$r_V A_1(0)$ $r_V = 1.463(35)$	2.112	$0.815^{+0.070}_{-0.051}$	2.007	1.059(124)	2.112

Table 11. Values of form factor parameters used in our analysis for the $P \to M$ transitions along with the reference from which they are taken.

where $F_i = A_1, A_2, A_0, V$ and $m_{R,i}$ are the respective pole masses. The kinematic constraint $A_0(0) = A_3(0) = (\frac{m_P+m_M}{2m_M} A_1(0) - \frac{m_P-m_M}{2m_M} A_2(0))$ relates the parameters at zero recoil. We list the values of the relevant parameters in Table. 11.

For the semileptonic baryonic decay, we employ the most recent lattice QCD computation of the form factors reported in [53]. There are a total of six form factors $f_+, f_\perp, f_0, g_+, g_\perp, g_0$ which are parameterized using a simple pole z-expansion of the form

$$f(q^2) = \frac{1}{1 - q^2/(m^f_{\text{pole}})^2} \sum_{n=0}^{n_{\max}} a_n^f \left[z(q^2) \right]^n, \tag{C.12}$$

where z is defined as in Eq. (C.3) with $t_0 = q^2_{\max} = (m_{\Lambda_c} - m_\Lambda)^2$ and $t_+ = (m_D + m_K)^2$. The pole masses are $m^{f_+,f_\perp}_{\text{pole}} = 2.112$ GeV, $m^{f_0}_{\text{pole}} = 2.318$ GeV, $m^{g_+,g_\perp}_{\text{pole}} = 2.460$ GeV and $m^{g_0}_{\text{pole}} = 1.968$ GeV. The "nominal fit" results for the form factor parameters provided in [53] have been used for our analysis.

References

[1] HFLAV collaboration, *Averages of b-hadron, c-hadron, and τ-lepton properties as of 2021*, *Phys. Rev. D* **107** (2023) 052008 [2206.07501].

[2] BaBar collaboration, *Evidence for an excess of $\bar{B} \to D^{(*)}\tau^-\bar{\nu}_\tau$ decays*, *Phys. Rev. Lett.* **109** (2012) 101802 [1205.5442].

[3] BaBar collaboration, *Measurement of an Excess of $\bar{B} \to D^{(*)}\tau^-\bar{\nu}_\tau$ Decays and Implications for Charged Higgs Bosons*, *Phys. Rev. D* **88** (2013) 072012 [1303.0571].

[4] LHCb collaboration, *Measurement of the ratio of branching fractions $\mathcal{B}(\bar{B}^0 \to D^{*+}\tau^-\bar{\nu}_\tau)/\mathcal{B}(\bar{B}^0 \to D^{*+}\mu^-\bar{\nu}_\mu)$*, *Phys. Rev. Lett.* **115** (2015) 111803 [1506.08614].

[5] Belle collaboration, *Measurement of the branching ratio of $\bar{B} \to D^{(*)}\tau^-\bar{\nu}_\tau$ relative to $\bar{B} \to D^{(*)}\ell^-\bar{\nu}_\ell$ decays with hadronic tagging at Belle*, *Phys. Rev. D* **92** (2015) 072014 [1507.03233].

[6] BELLE collaboration, *Measurement of the branching ratio of $\bar{B}^0 \to D^{*+}\tau^-\bar{\nu}_\tau$ relative to $\bar{B}^0 \to D^{*+}\ell^-\bar{\nu}_\ell$ decays with a semileptonic tagging method*, *Phys. Rev. D* **94** (2016) 072007 [1607.07923].

[7] BELLE collaboration, *Measurement of the τ lepton polarization and $R(D^*)$ in the decay $\bar{B} \to D^*\tau^-\bar{\nu}_\tau$*, *Phys. Rev. Lett.* **118** (2017) 211801 [1612.00529].

[8] LHCB collaboration, *Measurement of the ratio of the $B^0 \to D^{*-}\tau^+\nu_\tau$ and $B^0 \to D^{*-}\mu^+\nu_\mu$ branching fractions using three-prong τ-lepton decays*, *Phys. Rev. Lett.* **120** (2018) 171802 [1708.08856].

[9] BELLE collaboration, *Measurement of the τ lepton polarization and $R(D^*)$ in the decay $\bar{B} \to D^*\tau^-\bar{\nu}_\tau$ with one-prong hadronic τ decays at Belle*, *Phys. Rev. D* **97** (2018) 012004 [1709.00129].

[10] LHCB collaboration, *Test of Lepton Flavor Universality by the measurement of the $B^0 \to D^{*-}\tau^+\nu_\tau$ branching fraction using three-prong τ decays*, *Phys. Rev. D* **97** (2018) 072013 [1711.02505].

[11] BELLE collaboration, *Measurement of $\mathcal{R}(D)$ and $\mathcal{R}(D^*)$ with a semileptonic tagging method*, 1904.08794.

[12] LHCB collaboration, *Measurement of the ratios of branching fractions $\mathcal{R}(D^*)$ and $\mathcal{R}(D^0)$*, *Phys. Rev. Lett.* **131** (2023) 111802 [2302.02886].

[13] LHCB collaboration, *Test of lepton flavor universality using $B^0 \to D^{*-}\tau^+\nu_\tau$ decays with hadronic τ channels*, *Phys. Rev. D* **108** (2023) 012018 [2305.01463].

[14] BELLE-II collaboration, *A test of lepton flavor universality with a measurement of $R(D^*)$ using hadronic B tagging at the Belle II experiment*, 2401.02840.

[15] LHCB collaboration, *Measurement of the branching fraction ratios $R(D^+)$ and $R(D^{*+})$ using muonic τ decays*, 2406.03387.

[16] LHCB collaboration, *Measurement of the ratio of branching fractions $\mathcal{B}(B_c^+ \to J/\psi\tau^+\nu_\tau)/\mathcal{B}(B_c^+ \to J/\psi\mu^+\nu_\mu)$*, *Phys. Rev. Lett.* **120** (2018) 121801 [1711.05623].

[17] HFLAV collaboration, Y.S. Amhis et al., "Preliminary average of $R(D)$ and $R(D^*)$ for Moriond 2024." https://hflav-eos.web.cern.ch/hflav-eos/semi/moriond24/html/RDsDsstar/RDRDs.html, 2024.

[18] BELLE-II collaboration, *Evidence for $B^+ \to K^+\nu\bar{\nu}$ decays*, *Phys. Rev. D* **109** (2024) 112006 [2311.14647].

[19] HPQCD collaboration, *Standard Model predictions for $B \to K\ell^+\ell^-$, $B \to K\ell_1^-\ell_2^+$ and $B \to K\nu\bar{\nu}$ using form factors from $N_f = 2 + 1 + 1$ lattice QCD*, *Phys. Rev. D* **107** (2023) 014511 [2207.13371].

[20] LHCB collaboration, *Test of lepton universality in $b \to s\ell^+\ell^-$ decays*, *Phys. Rev. Lett.* **131** (2023) 051803 [2212.09152].

[21] B. Capdevila, A. Crivellin and J. Matias, *Review of semileptonic B anomalies*, *Eur. Phys. J. ST* **1** (2023) 20 [2309.01311].

[22] B. Bhattacharya, A. Datta, J.-P. Guévin, D. London and R. Watanabe, *Simultaneous Explanation of the R_K and $R_{D^{(*)}}$ Puzzles: a Model Analysis*, *JHEP* **01** (2017) 015 [1609.09078].

[23] B. Bhattacharya, A. Datta, D. London and S. Shivashankara, *Simultaneous Explanation of the R_K and $R(D^{(*)})$ Puzzles*, *Phys. Lett. B* **742** (2015) 370 [1412.7164].

[24] A. Rashed, M. Duraisamy and A. Datta, *Nonstandard interactions of tau neutrino via charged Higgs and W' contribution*, *Phys. Rev. D* **87** (2013) 013002 [1204.2023].

[25] A. Rashed, P. Sharma and A. Datta, *Tau neutrino as a probe of nonstandard interaction*, *Nucl. Phys. B* **877** (2013) 662 [1303.4332].

[26] H. Liu, A. Rashed and A. Datta, *Probing lepton nonuniversality in tau neutrino scattering*, *Phys. Rev. D* **92** (2015) 073016 [1505.04594].

[27] FASER collaboration, *Detecting and Studying High-Energy Collider Neutrinos with FASER at the LHC*, *Eur. Phys. J. C* **80** (2020) 61 [1908.02310].

[28] SND@LHC collaboration, *SND@LHC: the scattering and neutrino detector at the LHC*, *JINST* **19** (2024) P05067 [2210.02784].

[29] A. Falkowski, M. González-Alonso, J. Kopp, Y. Soreq and Z. Tabrizi, *EFT at FASERν*, *JHEP* **10** (2021) 086 [2105.12136].

[30] C. Ahdida et al., *SND@LHC - Scattering and Neutrino Detector at the LHC*, Tech. Rep. CERN-LHCC-2021-003, LHCC-P-016, CERN, Geneva (2021).

[31] D. Bečirević, F. Jaffredo, A. Peñuelas and O. Sumensari, *New Physics effects in leptonic and semileptonic decays*, *JHEP* **05** (2021) 175 [2012.09872].

[32] J. Kopp, N. Rocco and Z. Tabrizi, *Unleashing the Power of EFT in Neutrino-Nucleus Scattering*, 2401.07902.

[33] W. Buchmuller, R. Ruckl and D. Wyler, *Leptoquarks in Lepton - Quark Collisions*, *Phys. Lett. B* **191** (1987) 442.

[34] Y. Sakaki, M. Tanaka, A. Tayduganov and R. Watanabe, *Testing leptoquark models in $\bar{B} \to D^{(*)}\tau\bar{\nu}$*, *Phys. Rev. D* **88** (2013) 094012 [1309.0301].

[35] B. Bhattacharya, T.E. Browder, Q. Campagna, A. Datta, S. Dubey, L. Mukherjee et al., *Implications for the ΔAFB anomaly in $\bar{B}0 \to D^{*}+\ell\text{-}\nu^{-}$ using a new Monte Carlo event generator*, *Phys. Rev. D* **107** (2023) 015011 [2206.11283].

[36] S. Shivashankara, W. Wu and A. Datta, *$\Lambda_b \to \Lambda_c \tau \bar{\nu}_\tau$ Decay in the Standard Model and with New Physics*, *Phys. Rev. D* **91** (2015) 115003 [1502.07230].

[37] A. Datta, S. Kamali, S. Meinel and A. Rashed, *Phenomenology of $\Lambda_b \to \Lambda_c \tau \bar{\nu}_\tau$ using lattice QCD calculations*, *JHEP* **08** (2017) 131 [1702.02243].

[38] PARTICLE DATA GROUP collaboration, *Review of Particle Physics*, *PTEP* **2022** (2022) 083C01.

[39] FLAVOUR LATTICE AVERAGING GROUP (FLAG) collaboration, *FLAG Review 2021*, *Eur. Phys. J. C* **82** (2022) 869 [2111.09849].

[40] C. Bolognani, M. Reboud, D. van Dyk and K.K. Vos, *Constraining $|V_{cs}|$ and physics beyond the Standard Model from exclusive (semi)leptonic charm decays*, 2407.06145.

[41] F. James and M. Roos, *Minuit: A System for Function Minimization and Analysis of the Parameter Errors and Correlations*, *Comput. Phys. Commun.* **10** (1975) 343.

[42] H. Dembinski and P.O. et al., *scikit-hep/iminuit*, Dec, 2020. 10.5281/zenodo.3949207.

[43] F. Kling and L.J. Nevay, *Forward neutrino fluxes at the LHC*, *Phys. Rev. D* **104** (2021) 113008 [2105.08270].

[44] D. Abbaneo et al., *AdvSND, The Advanced Scattering and NeutrinoDetector at High Lumi LHC Letter of Intent*, Tech. Rep. CERN-LHCC-2024-007, LHCC-I-040, CERN, Geneva (2024).

[45] A. Datta and X. Zhang, *Nonuniversal correction to $Z \to b\bar{b}$ and single top quark production at Tevatron*, *Phys. Rev. D* **55** (1997) 2530 [hep-ph/9611247].

[46] R. Watanabe, *New Physics effect on $B_c \to J/\psi\tau\bar{\nu}$ in relation to the $R_{D^{(*)}}$ anomaly*, *Phys. Lett. B* **776** (2018) 5 [1709.08644].

[47] Belle collaboration, *Precise determination of the CKM matrix element $|V_{cb}|$ with $\bar{B}^0 \to D^{*+}\ell^-\bar{\nu}_\ell$ decays with hadronic tagging at Belle*, 1702.01521.

[48] ETM collaboration, *Scalar and vector form factors of $D \to \pi(K)\ell\nu$ decays with $N_f = 2 + 1 + 1$ twisted fermions*, *Phys. Rev. D* **96** (2017) 054514 [1706.03017].

[49] K. Azizi, R. Khosravi and F. Falahati, *Exclusive $D_s \to (\eta, \eta')l\nu$ decays in light cone QCD*, *J. Phys. G* **38** (2011) 095001 [1011.6046].

[50] BaBar collaboration, *Analysis of the $D^+ \to K^-\pi^+e^+\nu_e$ decay channel*, *Phys. Rev. D* **83** (2011) 072001 [1012.1810].

[51] H.-B. Fu, L. Zeng, R. Lü, W. Cheng and X.-G. Wu, *The $D \to \rho$ semileptonic and radiative decays within the light-cone sum rules*, *Eur. Phys. J. C* **80** (2020) 194 [1808.06412].

[52] HPQCD collaboration, *V_{cs} from $D_s \to \phi\ell\nu$ semileptonic decay and full lattice QCD*, *Phys. Rev. D* **90** (2014) 074506 [1311.6669].

[53] S. Meinel, *$\Lambda_c \to \Lambda l^+\nu_l$ form factors and decay rates from lattice QCD with physical quark masses*, *Phys. Rev. Lett.* **118** (2017) 082001 [1611.09696].